Noname manuscript No.
(will be inserted by the editor)

Radiographic Reconstruction of Osteotomized Bone Fragments: A First Trial

Steffen Schumann · Richard Bieck · Rainer Bader · Paul A. Grützner · Johannes Heverhagen · Lutz-P. Nolte · Guoyan Zheng

Received: date / Accepted: date

Abstract *Purpose* The correct rotational alignment of a fractured long bone is an important step in the fracture reduction process. In order to plan the fracture reduction and the appropriate external fixation, plain radiographs are conventionally used. But as three-dimensional information of the complex situation is not available, the correct amount of rotation can only be approximated. Thus, the objective of this study is to develop a system to assess the rotational relationship between proximal and distal fragments of the tibia and femur based on a set of two calibrated X-ray radiographs.

Methods In order to robustly determine the rotational alignment of proximal and distal bone fragments, a 2D/3D reconstruction approach was employed to reconstruct the fractured bone fragments. Two different studies were performed to evaluate the accuracy of the complete system for the purpose of fracture reduction.

Results The reconstruction accuracy was evaluated in terms of major bone axis and in-plane rotational alignment. The long bone axis of the femur and tibia could be derived an average with an error of $0.33 \pm 0.27^{\circ}$, while an average in-plane rotational error of $2.27 \pm 1.76^{\circ}$and $2.67 \pm 1.80^{\circ}$was found for the proximal

S. Schumann · L.P. Nolte · G. Zheng
Institute for Surgical Technology and Biomechanics (ISTB)
University of Bern, Bern, Switzerland
Tel.: +41-31-6315949
E-mail: steffen.schumann@ieee.org, E-mail: guoyan.zheng@ieee.org

R. Bieck · R. Bader
Biomechanics and Implant technology research laboratory
Department of Orthopaedics
University of Rostock, Rostock, Germany

P.A. Grützner
BG Trauma Centre Ludwigshafen at Heidelberg University Hospital
Ludwigshafen, Germany

J. Heverhagen
Department of Radiology, Inselspital
University of Bern, Bern, Switzerland

and distal fragment, respectively. The overall mean surface reconstruction error of tibial fragments was 0.81 ± 0.59 mm and 1.12 ± 0.87 mm for femoral fragments.

Conclusions A new approach for estimating the rotational parameters of fractured bone fragments has been proposed. This approach is based on two conventional radiographs and 2D/3D reconstruction technology. It is generally applicable to the reduction of any simple long bone fracture and could provide an important means for external fracture fixations.

Keywords long bone · tibia · femur · reconstruction · osteotomy · radiographic · Ilizarov · Taylor Spatial Frame

1 Introduction

The alignment of fractured fragments is an essential step in the surgical treatment of long bone fractures. A malalignment of the fragments can lead to an insufficient fracture healing and a loss of limb function [1]. Fractures of long bones are commonly reduced with distraction osteogenesis using external fixators [2], [3], [4]. A nowadays widely-used concept for distraction osteogenesis was developed by Gavriil A. Ilizarov [5]. He invented a circular external fixator to constantly apply tension stress to the bone to stimulate its regeneration. An advancement of this system, the Taylor Spatial Frame (Smith & Nephew, Memphis, USA) enables multidirectional deformity correction [6], [7], [8]. One of the prerequisites for a successful treatment using an external fixator is the correction of the malaligned bone fragments [1]. During such a distraction phase, the patients need to undergo recurrent X-ray image acquisitions [9]. As only two-dimensional (2D) image information is available, the actual limb alignment cannot be accurately assessed [10], [11]. In order to assess the limb alignment in all three dimensions (3D), a suitable imaging modality such as computed-tomography (CT) or magnetic resonance imaging (MRI) would need to be used. However, an application of these 3D imaging modalities could not be justified, as the recurrent examinations are associated with a repetitive exposure of radiation and high costs. Thus, 2D/3D reconstruction methods based on statistical shape models (SSMs) could be a valuable alternative. Methods for 2D/3D reconstruction of the femur and tibia from X-ray radiographs were presented by Messmer et al. [12], Gunay et al. [13], Gamage et al. [14] and Quijano et al. [15]. All approaches perform a 3D reconstruction of the intact bone and are therefore not directly applicable to the reconstruction of a fractured bone. In clinical practice the X-ray radiography gives only information on the bone in the fractured status. Consequently, the actual relationship between the proximal and distial bone fragments is not known. In order to reduce the fracture and to properly align both the fragments, the major long bones axis needs to be restored and the rotation around this axis needs to be identified.

The contribution of this work is twofold. (1) In order to assess the rotational alignment of the bone fragments, 2D/3D registration technique is employed to reconstruct surface models of the proximal and distal fragments from a set of conventional X-ray radiographs. We will present the adapted 2D/3D reconstruction framework [16] for extracting patient-specific surface models of fractured femur and tibia bones from biplanar radiographs. (2) Two studies were performed to validate the accuracy of the overall system. Digitally reconstructed radiographs

(DRRs) were used in the first study to compute the reconstruction accuracy, while a customized mockup and conventional radiography was used in the second study to evaluate the accuracy of our proposed method.

2 Materials & Methods

2.1 Statistical Femur & Tibia Model

For 3D reconstruction of a patient-specific model of the tibial fracture, the concept of statistical shape models (SSMs) [17] is employed. Computed tomography (CT) scans of intact tibial and femoral bones were semi-automatically segmented using Amira software (FEI, Hillsboro, USA) and correspondences between the models were determined by non-rigid mesh registration [18]. Thereby, a reference volume was selected and the remaining floating volumes were non-rigidly registered using diffeomorphic demons algorithm [19]. For each resulting deformation field, the reference surface model was accordingly warped to recover the shape of the floating instances. By this step, the correspondences among the training instances were established and the shape variation could be extracted using Principal Component Analysis (PCA). The statistical population consisted of 17 tibial and 129 femoral instances.

2.2 2D/3D Reconstruction

The 2D/3D reconstruction of the bone fragments is based on a previously developed methodology [16]. This methodology was originally developed for the reconstruction of the proximal femur, but can be applied for the reconstruction of any other bone. It requires a set of minimum two calibrated X-ray images and a SSM of the particular bone to be reconstructed. Based on a set of anatomical landmarks and 2D bone contours, the SSM is iteratively fit to these extracted features. Upon convergence, the SSM is instantiated based on its intrinsic statistical information. A final non-rigid deformation step is applied to optimally reconstruct the underlying bone geometry. For more details of this algorithm we would like to refer to this work [16].

As the methodology of 2D/3D reconstruction follows general principles, it can be also adapted to reconstruct fractured femur and tibia bones. The set of X-ray images is composed of an anterior-posterior (AP) and a lateral view of the particular bone. The calibration is accomplished by integrating a small-sized calibration unit into the acquisition process [20]. In order to initially match the SSM of the respective bone to the radiographs, the mean model needs to be split up into two independent fragments according to the present fracture. The proximal and distal fragment lengths are estimated with respect to the length of the complete intact bone, by indicating a value between 0.0 and 1.0. A value of 0.5 indicates an approximately equal length of both fragments (fracture site at the bone center), while values larger (smaller) than 0.5 indicate a larger proportion of the proximal (distal) fragment. Based on this value the intact bone SSM is split into two fragments, whereas the length of the main bone axis is taken as a reference measure. As the SSM consists of a population of aligned surface models, each model can be

Table 1 Anatomical landmarks which need to be defined for initial landmark-based registration of SSMs.

		tibia	femur
proximal	(1)	center of medial and lateral intercondylar tubercle	apex of greater trochanter
	(2)	most medial point of the tibial plateau	femoral head center
	(3)	most lateral point of the tibial plateau	apex of lower trochanter
distal	(1)	center of medial malleolus and incisura fibularis	intercondylar notch
	(2)	apex medial malleolus	medial epicondyle
	(3)	center of incisura fibularis	lateral epicondyle

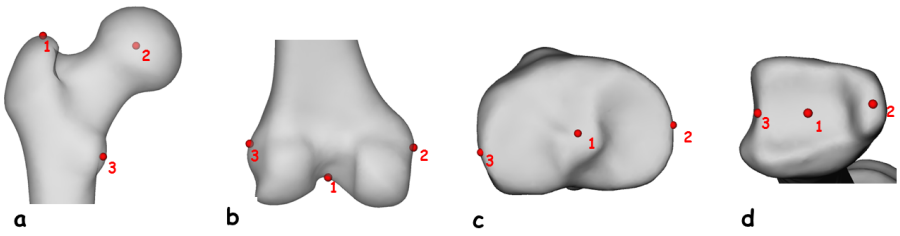

Fig. 1 a), b) Landmarks of proximal and distal femur (left femur). The femoral head center is determined by fitting a sphere to the vertices of the surface model; c), d) Tibial landmarks of proximal and distal plafond (left tibia). The lateral and medial landmarks of both tibial parts are defined based on the point of maximum curvature.

split into two parts according to the indicated percentage value. Thereby, it is not important to exactly match the length of the fractured fragments. We are mainly interested in the rotational arrangement of the fragments and not in the precise fragment length or the appearance of the fracture site. Both bone fragments are then independently matched to the radiographic scene based on the methodology introduced in [16].

In the first step five pre-defined landmarks were picked for each fragment on both radiographs. For each fragment two of the five points were picked along the main bone axis, whereas the exact location is not of importance as they are solely used to determine the main axis. The remaining three points correspond to specific anatomical landmarks, which need to be defined in order to match the SSMs to the radiographic scene. These landmarks are commonly used in literature [21], [22], [23] and are depicted in Fig. 1. As the identification of the anatomical landmarks in the lateral view is slightly more difficult, epipolar lines are visualized on the lateral image for each landmark identified in the AP image. Consequently, the identification of the landmark could be constrained to the particular epipolar line. As the same landmarks were also predefined on the intact mean model in SSM-space, a matching was achieved by superimposing the identified points and the main bone axis with the corresponding points and axis of the SSM fragments. Thereby, the main tibia axis is defined by center of the intercondylar tubercles

(landmark (1) of proximal tibia) the and the medial malleolus apex (landmark (1) of distal tibia). The main femoral axis is defined by the greater trochanter apex (landmark (1) of proximal femur) and the intercondylar notch (landmark (1) of distal femur). In a next step, 2D image contours of both fragments were drawn using a semi-automatic method. The contours are drawn along the bone edges, whereas the fracture site is omitted. The remaining steps were performed as described in [16]: The model fragments were first iteratively fit to the image scene, instantiated and then non-rigidly deformed to recover the shape of the underlying bone fragments.

3 Experimental Validation

As part of this experimental validation, two studies were conducted to evaluate the accuracy of our proposed method. In a first study, digitally reconstructed radiographs (DRRs) of virtually fractured femur and tibia bones were used to validate the proposed approach. In a second study, a mockup phantom was constructed to simulate different tibial fractures. Conventional radiographs of different configurations were acquired and compared to the ground truth CT-scans. For both studies the 2D/3D reconstruction accuracy in terms of surface error and rotational alignment error was assessed.

3.1 Experimental Validation using DRRs

In this first study, CT-datasets of cadaveric specimens were segmented using Amira software and surface models of the femur and tibia were extracted. For each segmented model, ground truth landmarks as defined in Table 1 were manually defined. Moreover, three different fracture levels were simulated for each bone by splitting the CT-volume into two halfs. The three levels were approximately in both metaphysis regions (proximal and distal) and at the center of the diaphysis. In oder to test different fracture scenarios, an arbitrary transformation was applied to the distal half of the split CT-volume. This composed CT-volume was further used to generate two DRRs in AP and lateral view (camera parameters?). Subsequently, the DRRs with corresponding calibration information were used for 2D/3D reconstruction as described in section 2.2. The reconstructed models were consequently in the same space as the ground truth models. A set of DRRs and reconstructed models is shown in Fig. 2. The actual data analysis is described in section 3.3, whereas a summary of all involved steps is shown in Fig. 5.

3.2 Experimental Validation using Mockup Phantom

In this second study, conventional radiographs were acquired of a customized mockup. This mockup was designed and constructed for the purpose of simulating various fracture scenarios. It provides a separate fixation for two plastic bone fragments and allows to freely adjust both fragments (see Fig. 3). While the proximal fragment is rigidly attached to a fixation block which can be varied in its height and distance on the base plate, the distal fragment is connected to the

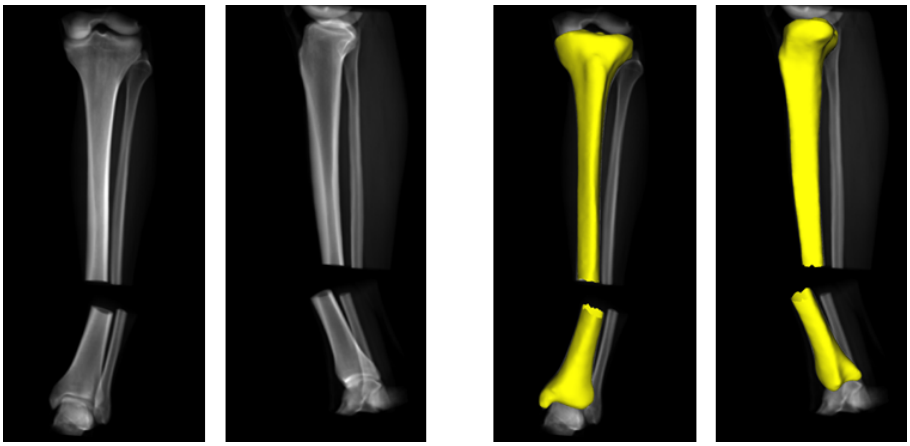

Fig. 2 Set of digitally reconstructed radiographs (left) and with reconstructed fragments superimposed (right).

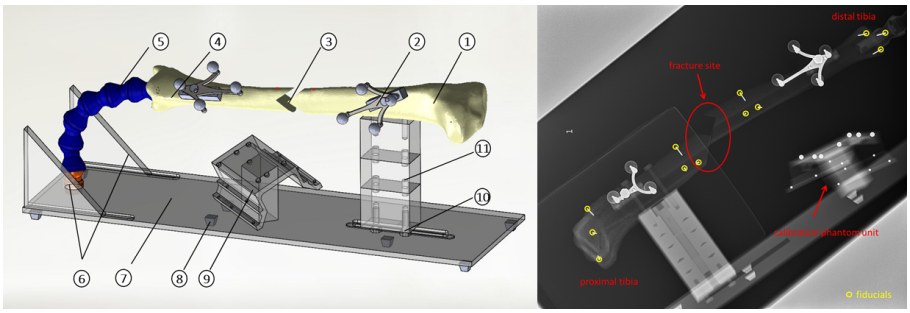

Fig. 3 Left: Drawing of the constructed mockup: 1 - proximal bone fragment, 2 - proximal dynamic reference base (not used for this study), 3 - fracture site, 4 - distal bone fragment, 5 - modular positioning arm, 6 - vertical positioning support, 7 - base plate, 8 - anti slip posts, 9 - calibration unit, 10 - horizontal adjustment, 11 - vertical adjustment; Right: X-ray radiograph of customized mockup in lateral view. The circles indicate the fiducials as listed in Table 2.

.

base plate via a modular hose system (Lockwood Products Inc., Lake Oswego, United States). The hose system enables a nearly unrestricted spatial positioning of the distal bone fragment with respect to the proximal bone fragment as well as 360° of rotation around the main tibial axis. Moreover, the calibration unit was rigidly attached the base plate. All the mockup components were made out of plastic material (PMMA) to preserve radiolucent properties of the whole setup. Six nail fiducials with tiny indents were inserted into each bone fragment for the accuracy analysis. The exact fiducial locations are summarized in Table 2. The mockup was consecutively equipped with fragments of two different tibial plastic bones. Both plastic bones were artificially fractured by sawing a wedge-shaped fracture site into the diaphysis. For the first bone the fracture-site was laterally oriented and more proximally (see Fig. 3), while the fracture-site of the second bone was more distally and in anterior-posterior direction. After mounting each bone to the mockup, the fragments were realigned and fixed, recovering the original intact tibia bone for

Table 2 Anatomical location of fiducials inserted into both fragments of each tibia bone model.

proximal fragment

proximal	distal
tuberositas tibia	margo interosseous
lateral tibia plateau edge	margo anterior
medical tibia plateau edge	margo medialis

distal fragment

proximal	distal
margo interosseous	apex malleolus medialis
margo anterior	anterior end of incisura fibularis
margo medials	posterior end of incisura fibularis

acquisition of a ground truth CT-scan (Somatom, Siemens, Erlangen, Germany). The CT-datasets of both bones were semi-automatically segmented using Amira software, resulting in ground truth model fragments. Moreover, the nail fiducials were identified by manually localizing the fiducial center in the respective CT stack. Thereupon the fragments were manually put into five different configurations, simulating different tibial fracture adjustments. For each configuration two X-ray radiographs (AP and lateral view) were acquired (s. Fig. 3) and consequently calibrated. The set of calibrated radiographs was used to reconstruct the proximal and distal fragments. In addition, the projected nail fiducials were identified in both views and triangulated to unique 3D positions. Pair-point matching was performed to align the ground truth fragments with the particular fracture configuration in X-ray space. Thus, corresponding nail fiducials were used to compute the respective transformation. Upon alignment, the data were further analysed as described in section 3.3.

3.3 Subjective-free Validation

In order to analyse the surface reconstruction accuracy in both studies, a rigid alignment for each pair of models was conducted. Hence, each ground truth fragment was registered to its reconstructed counterpart. As the length of the reconstructed fragments was not exactly equal to the actual ground truth length, both models were cropped at the same level near the fracture site. The surface reconstruction error was then computed between the pair of equally cropped fragments. The rotational alignment error was assessed based on the ground truth and reconstructed landmarks. As the reconstructed model is subject to certain small distortions during the non-rigid registration process, landmarks could not be taken over from the original statistical mean model and thus would need to be redefined. To avoid subjective interactive landmark picking on the reconstructed models, these landmarks were defined by non-rigid registration of the ground truth models: Firstly, both cropped surface models are transformed to binary volumes using Amira software. Subsequently, diffeomorphic demons algorithm [19] is used to non-rigidly deform the ground truth volume with respect to the reconstructed volume. The computed displacement vector field is then applied to the ground truth landmarks, which have been updated by the rigid transformation ${}_{frag}T_{rec}^{GT}$

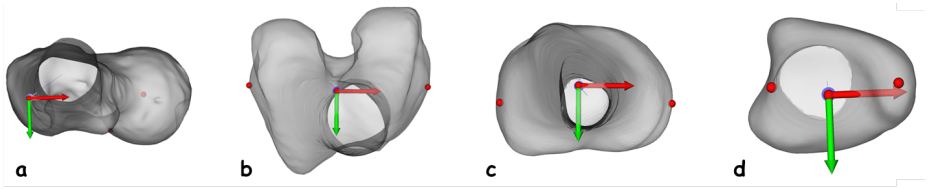

Fig. 4 Definition of coordinate-systems for left femur and tibia bones. The proximal parts (a, c) are shown in cranial-caudal direction, while the distal parts (b, d) are shown in caudal-cranial direction.

(s. step (6) in Fig. 5). The resulting landmark positions are further adjusted to correspond to the closest vertex on the reconstructed model, resulting in the actually reconstructed landmarks. In order to determine the reconstruction accuracy of the main long bone axis, the pair of reconstructed fragments were aligned to recover the intact bone configuration. Thereby, the ground truth transformation of the distal fragment from intact to fractured state was inverted and applied to the reconstructed distal fragment.

The landmarks are further used to set up unique coordinate-systems for the proximal and distal fragment (s. Fig. 4). The origins of the coordinate-systems (COSs) are defined by the particular (1)-landmarks (s. Tab. 1). The z-axes are defined by connecting both proximal and distal (1)-landmarks, whereas this common line also represents the main long bone axis. Thereby, the z-axis of the proximal COS points caudally, while the z-axis of the distal COS points cranially. The proximal femur x-axis is defined by the origin and the femoral head center landmark, while the remaining x-axes are defined by projecting the line out of landmarks (2) and (3) onto an plane defined by landmark (1) (plane position) and the main long bone axis (plane normal). For each COS, the x-axis points medially (red axis in Fig. 4). The y-axis is derived by the cross-product of defined z- and x-axis. The proximal y-axes point in anterior-posterior direction, while the distal y-axes are in posterior-anterior direction. The comparison of the ground truth COSs with the reconstructed COSs is decomposed into two error measurements. The axis alignment error (AAE) is measured as the angle difference of the main long bone axis between the ground truth fragments and the reconstructed fragments. The in-plane rotation error (IRE) describes the bone fragments' rotation error of the proximal COS in relation to its corresponding distal COS around the main long bone axis. Thus, the IRE measures the alignment discrepancy within the transversal plane. A summary of all the involved steps of accuracy analysis is also shown in Fig. 5.

4 Results

4.1 Results of DRR-Study

Six femoral CT-datasets and six tibial CT-datasets were used in the DRR-study. For each CT-dataset, three differently fractured volumes were generated, resulting in 36 datasets in total. The respective CT-datasets were not part of the population, used to generate the statistical models. In the first step, the surface reconstruction

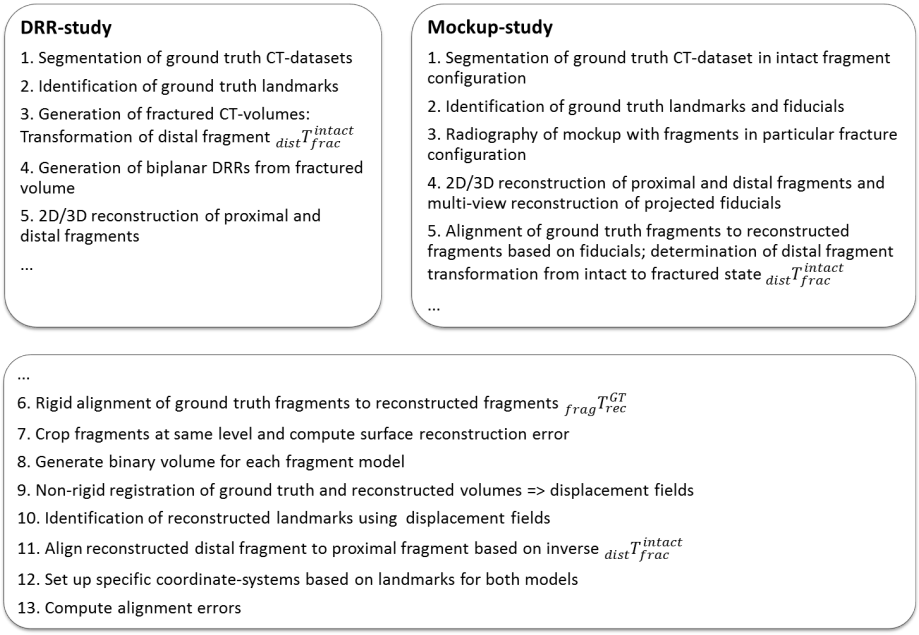

Fig. 5 Series of steps carried out to analyse the accuracy of the proposed system for both studies. Steps (6) to (13) are carried out for both studies.

error was computed. On average, the proximal tibia fragment was reconstructed with an error of 0.88 ± 0.63 mm and the distal tibia fragment with an error of 0.78 ± 0.56 mm. The surface reconstruction error of the femoral fragments was slightly increased. An error of 1.12 ± 0.89 mm was observed for the proximal fragment, while the distal fragment was reconstructed with an error of 1.13 ± 0.84 mm. The axis alignment error (AAE) was relatively robust throughout all 36 cases. For the tibia reconstructions, an average AAE of 0.24 ± 0.17° (maximum error of 0.80°) was found, while the average AAE was 0.25 ± 0.14° (maximum error of 0.80°) for the femur reconstructions. The average in-plane rotation error (IRE) was independently assessed for the proximal and distal fragments. The IRE of the proximal tibia fragments was 3.08 ± 2.01° (maximum error of 7.65°) and 3.16 ± 2.02° (maximum error of 7.53°) for the distal tibia fragments. In contrast to the surface reconstruction error, the IRE was improved for the femoral fragments. 1.32 ± 0.95° (max. error 3.22°) was measured for the proximal IRE and 2.71 ± 1.69° (max. error of 6.61°) for the distal IRE. The individual contributions to the average error are shown in Fig. 6.

4.2 Results of Mockup-Study

Two different tibial bone models were used to simulate ten different fracture scenarios (five for each model). The average surface reconstruction error of the proximal fragment was 0.71 ± 0.59 mm (0.74 ± 0.60 mm for the first tibia model and 0.68 ± 0.57 mm for the second tibia model). The average surface reconstruction

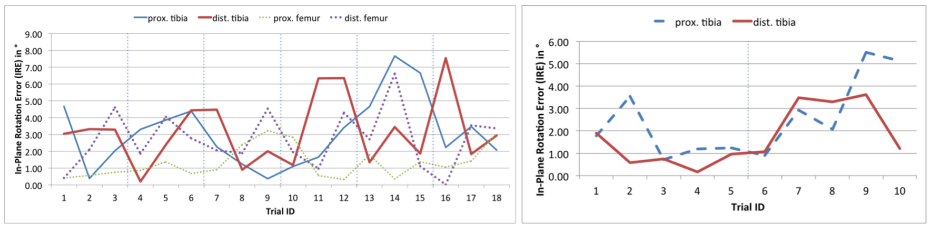

Fig. 6 Left: In-plane rotation errors of DRR-study. The femoral IREs are depicted by dotted lines. Three successive trials belong to the same bone; Right: In-plane rotation error of the mockup study. The first five cases belong to the first tibia model, the second five cases to the second tibia model. The prox. tibia IRE is depicted by a discontinuous line.

error of the distal fragment was 0.78 ± 0.67 mm and thus in a similar range as for the proximal fragment. For the first tibia model the error was 0.79 ± 0.66 mm and for the second bone 0.77 ± 0.69 mm. Major inaccuracies were distributed around the tibial plateau and the plafond area. Thereby, prominent bone edges such as *malleolus medialis* or the *eminentia intercondylaris* showed the highest errors.

The AAE of the main tibial axis was on average 0.48 ± 0.38°(0.41± 0.25° for the first tibia model and 0.36 ± 0.87° for the second tibia model). The IRE observed for the proximal fragment was 2.50 ± 1.73° (1.69 ± 1.10° for the first model and 3.31 ± 1.97°for the second model), and 1.70 ± 1.30° (0.87 ± 0.64°for the first tibia and 2.54 ± 1.28°for the second tibia) for the distal fragment. Maximum errors of 5.50°and 5.12° were measured for two trials of the second proximal model, slightly exceeding the clinically acceptable error of 5°. The contribution of each trial to this average in-plane roration error is shown in Fig. 6.

5 Discussion

The correct alignment of fractured bone fragments is a crucial step in the surgical treatment of bone fractures. The alignment during the fracture healing process is monitored by the acquisition of X-ray radiographs at regular intervals. As only 2D information is available, the assessment of the actual 3D fracture reduction is limited. For a precise planning of deformity correction and fracture reduction it is important to have a 3D model of the fractured case. In order to assess the alignment of long bone fragments in all three dimensions, we developed a robust method to describe the rotational relationship between proximal and distal fragments based on biplanar plain radiographs. A SSM based 2D/3D reconstruction algorithm was adapted to reconstruct patient-specific fractured femoral and tibial bones. Two studies based on DRRs and conventional X-ray radiographs were conducted to evaluate the accuracy of the proposed approach.

The mean surface reconstruction error of all trials (18+10 tibial fragment reconstructions 18 femoral fragment reconstructions) was 1.12 ± 0.87 mm for the femoral fragments and 0.80 ± 0.61 mm for the tibial fragments. Major errors were thereby found at the greater trochanter and the tibial plafond area. In comparison to other existing works on 2D/3D femur and tibia reconstruction, the presented surface reconstruction errors are considerably lower. While Messmer et al. [12] achieved average errors of 1.5 ± 0.70 mm for the tibial shaft, 2.2 ± 0.79 mm for

the tibial plateau and 2.4 ± 0.82 mm for the plafond area, Quijano et al. [15] reported a mean reconstruction error of 1.3 mm.

Besides the surface reconstruction error, the geometrical error was assessed in terms of major bone axis alignment and transversal in-plane rotation difference. With the proposed method, the long bone axis could be derived with a 3D angular error of 0.33 ± 0.27°. The rotational error around this long bone axis was on average 2.27 ± 1.76°for the proximal bone fragments and 2.67 ± 1.80°for the distal bone fragments. The reconstruction of the major axis was generally robust, while the rotational error around this axis was slightly increased. This observation can be explained by the 2D/3D reconstruction process. While a tight fitting of the SSM to the outer contours is always achieved, certain rotations around this main longitudinal axis cannot be fully recovered from two views.

We also have to acknowledge certain limitations of the presented method. As it is only applicable to simple fractures, it cannot be applied to comminuted fractures. Moreover, an explicit reconstruction of the fracture site and the correct bone fragment length was not considered. It was also found that the 3D reconstruction of the bone fragments is very sensitive to the correct identification of the landmarks. A misplaced landmark could lead to a certain rotational reconstruction error. This is due to the fact that only the proximal and distal ends of a long bone have prominent features to control the registration around its longitudinal axis. Another limitation of our study is the relatively small statistical training population of the tibial statistical model and the low cases of specimens. Thus, more data needs to be gathered to draw a clinically meaningful conclusion.

The proposed concept of deriving the axial and rotational relationship of simple bone fragments could be applied to any long bone. Thus, the spatial transformation between major bone fragments could be always quantitatively determined. Moreover, the proposed system of 2D/3D reconstruction and fracture alignment has the potential to reduce the number of recurrent X-ray radiograph acquisitions.

Acknowledgements The authors would like to thank Alper Akcöltekin, Urs Rohrer and the team from the machine shop for the valuable support in conducting this study.

6 Conflict of Interest

The authors have no conflict of interest related to this work.

References

1. A Kanellopoulos and P Soucacos. Management of nonunion with distraction osteogenesis. *Injury*, 37(1):S51–S55, 2006.
2. D Paley, MA Catagni, F Argnani, A Villa, GB Bijnedetti, and R Cattaneo. Ilizarov treatment of tibial nonunions with bone loss. *Clinical orthopaedics and related research*, 241:146–165, 1989.
3. H Tsuchiya and K Tomita. Distraction osteogenesis for treatment of bone loss in the lower extremity. *Journal of orthopaedic science*, 8(1):116–124, 2003.
4. JJ GugenheimJr and MR Brinker. Bone realignment with use of temporary external fixation for distal femoral valgus and varus deformities. *The Journal of Bone & Joint Surgery*, 85(7):1229–1237, 2003.
5. GA Ilizarov. Clinical application of the tension-stress effect for limb lengthening. *Clinical orthopaedics and related research*, 250:8–26, 1990.

6. David S Feldman, Steven S Shin, Sanjeev Madan, and Kenneth J Koval. Correction of tibial malunion and nonunion with six-axis analysis deformity correction using the taylor spatial frame. *Journal of orthopaedic trauma*, 17(8):549–554, 2003.
7. Mohamed Fadel and Gamal Hosny. The taylor spatial frame for deformity correction in the lower limbs. *International orthopaedics*, 29(2):125–129, 2005.
8. Hans Michael Manner, Michael Huebl, Christof Radler, Rudolf Ganger, Gert Petje, and Franz Grill. Accuracy of complex lower-limb deformity correction with external fixation: a comparison of the taylor spatial frame with the ilizarov ring fixator. *Journal of children's orthopaedics*, 1(1):55–61, 2007.
9. D Paley. Progress in and from limb lengthening.
10. A Durandet, P-L Ricci, AH Saveh, Q Vanat, B Wang, I Esat, and M Chizari. Radiographic analysis of lower limb axial alignments. In *Proceedings of the World Congress on Engineering*, volume 2, 2013.
11. JP Cobb, H Dixon, W Dandachli, and F Iranpour. The anatomical tibial axis reliable rotational orientation in knee replacement. *Journal of Bone & Joint Surgery, British Volume*, 90(8):1032–1038, 2008.
12. P Messmer, G Long, N Suhm, P Regazzoni, and AL Jacob. Volumetric model determination of the tibia based on 2d radiographs using a 2d/3d database. *Computer Aided Surgery*, 6(4):183–194, 2001.
13. M Gunay, M-B Shim, and K Shimada. Cost- and time-effective three-dimensional bone-shape reconstruction from x-ray images. *The International Journal of Medical Robotics and Computer Assisted Surgery*, 3(4):323–335, 2007.
14. Pavan Gamage, Sheng Quan Xie, Patrice Delmas, and Wei Liang Xu. Diagnostic radiograph based 3d bone reconstruction framework: Application to the femur. *Computerized Medical Imaging and Graphics*, 35(6):427–437, 2011.
15. S Quijano, A Serrurier, B Aubert, S Laporte, P Thoreux, and W Skalli. Three-dimensional reconstruction of the lower limb from biplanar calibrated radiographs. *Medical engineering & physics*, 35(12):1703–1712, 2013.
16. G Zheng and S Schumann. 3d reconstruction of a patient-specific surface model of the proximal femur from calibrated x-ray radiographs: A validation study. *Medical physics*, 36(4):1155–1166, 2009.
17. TF Cootes, CJ Taylor, DH Cooper, and J Graham. Active shape models-their training and application. *Computer vision and image understanding*, 61(1):38–59, 1995.
18. G Heitz, T Rohlfing, and Calvin R Maurer Jr. Statistical shape model generation using nonrigid deformation of a template mesh. In *Medical Imaging*, pages 1411–1421. International Society for Optics and Photonics, 2005.
19. T Vercauteren, X Pennec, A Perchant, and N Ayache. Diffeomorphic demons: Efficient non-parametric image registration. *NeuroImage*, 45(1):S61–S72, 2009.
20. S Schumann, B Thelen, S Ballestra, LP Nolte, P Büchler, and G Zheng. X-ray image calibration and its application to clinical orthopedics. *Medical engineering & physics*, 36(7):968–974, 2014.
21. J Victor, D Van Doninck, L Labey, B Innocenti, PM Parizel, and J Bellemans. How precise can bony landmarks be determined on a ct scan of the knee? *The Knee*, 16(5):358–365, 2009.
22. K Subburaj, B Ravi, and M Agarwal. Automated identification of anatomical landmarks on 3d bone models reconstructed from ct scan images. *Computerized Medical Imaging and Graphics*, 33(5):359–368, 2009.
23. G Wu, S Siegler, P Allard, C Kirtley, A Leardini, D Rosenbaum, M Whittle, DD DLima, L Cristofolini, H Witte, O Schmid, and I Stokes. Isb recommendation on definitions of joint coordinate system of various joints for the reporting of human joint motionpart i: ankle, hip, and spine. *Journal of biomechanics*, 35(4):543–548, 2002.
24. SW Looney and TR Gulledge. Use of the correlation coefficient with normal probability plots. *The American Statistican*, 39:75–79, 1985.